HHS Public Access

Author manuscript

Cell Immunol. Author manuscript; available in PMC 2024 September 11.

Published in final edited form as:

Cell Immunol. 2024 ; 403-404: 104860. doi:10.1016/j.cellimm.2024.104860.

R406 reduces lipopolysaccharide-induced neutrophil activation

Seth Warner[a,b], **Heather L. Teague**[a,b], **Marcos J. Ramos-Benitez**[c], **Sumith Panicker**[d], **Kiana Allen**[a,b], **Salina Gaihre**[a,b], **Tom Moyer**[e], **Bindu Parachalil Gopalan**[f], **Iyadh Douagi**[e,g], **Arun Shet**[f], **Yogendra Kanthi**[d], **Anthony F. Suffredini**[a,b], **Daniel S. Chertow**[a,b,h], **Jeffrey R. Strich**[a,b,*]

[a]Critical Care Medicine Branch, National Heart, Lung, and Blood Institute, National Institutes of Health, Bethesda, MD, USA

[b]Critical Care Medicine Department, National Institutes of Health Clinical Center, National Institutes of Health, Bethesda, MD, USA

[c]Basic Science Department, Microbiology Division, School of Medicine, Ponce Health Sciences University, Ponce, PR, USA

[d]Laboratory of Vascular Thrombosis and Inflammation, National Heart, Lung, and Blood Institute, National Institutes of Health, Bethesda, MD, USA

[e]Flow Cytometry Section, Research Technologies Branch, National Institute of Allergy and Infectious Diseases, National Institutes of Health, Bethesda, MD, USA

[f]Laboratory of Sickle Thrombosis and Vascular Biology, National Heart, Lung, and Blood Institute, National Institutes of Health, Bethesda, MD, USA

[g]NIH Center for Human Immunology, Inflammation, and Autoimmunity, National Institute of Allergy and Infectious Diseases, National Institutes of Health, Bethesda, MD, USA

[*]Corresponding author at: Critical Care Medicine Department, National Institutes of Health Clinical Center, 10 Center Drive B10, 2C145, Bethesda, MD 20892, USA. jeffrey.strich@nih.gov (J.R. Strich).

5. Disclaimer

The opinions expressed in this article are those of the authors and do not represent any position or policy of the National Institutes of Health, the US Department of Health and Human Services, or the US government.

CRediT authorship contribution statement

Seth Warner: Writing – review & editing, Writing – original draft, Methodology, Investigation, Formal analysis, Data curation, Conceptualization. **Heather L. Teague:** Writing – review & editing, Writing – original draft, Formal analysis, Data curation, Conceptualization. **Marcos J. Ramos-Benitez:** Writing – review & editing, Formal analysis, Conceptualization. **Sumith Panicker:** Writing – review & editing, Investigation, Formal analysis, Data curation. **Kiana Allen:** Writing – review & editing, Formal analysis, Data curation, Conceptualization. **Salina Gaihre:** Writing – review & editing, Formal analysis, Data curation. **Tom Moyer:** Writing – review & editing, Data curation, Conceptualization. **Bindu Parachalil Gopalan:** Writing – review & editing, Data curation, Conceptualization. **Iyadh Douagi:** Writing – review & editing, Data curation, Conceptualization. **Arun Shet:** Formal analysis, Data curation, Conceptualization. **Yogendra Kanthi:** Writing – review & editing, Writing – original draft, Formal analysis, Data curation. **Anthony F. Suffredini:** Writing – review & editing, Writing – original draft, Conceptualization. **Daniel S. Chertow:** Writing – review & editing, Supervision, Funding acquisition, Formal analysis, Data curation, Conceptualization. **Jeffrey R. Strich:** Writing – review & editing, Writing – original draft, Supervision, Investigation, Funding acquisition, Formal analysis, Data curation, Conceptualization.

Declaration of competing interest

The authors declare that they have no known competing financial interests or personal relationships that could have appeared to influence the work reported in this paper.

Appendix A. Supplementary data

Supplementary data to this article can be found online at https://doi.org/10.1016/j.cellimm.2024.104860.

[h]Laboratory of Virology, National Institute of Allergy and Infectious Diseases, National Institutes of Health, Bethesda, MD, USA

Abstract

Modulating SYK has been demonstrated to have impacts on pathogenic neutrophil responses in COVID-19. During sepsis, neutrophils are vital in early bacterial clearance but also contribute to the dysregulated immune response and organ injury when hyperactivated. Here, we evaluated the impact of R406, the active metabolite of fostamatinib, on neutrophils stimulated by LPS. We demonstrate that R406 was able to effectively inhibit NETosis, degranulation, ROS generation, neutrophil adhesion, and the formation of $CD16^{low}$ neutrophils that have been linked to detrimental outcomes in severe sepsis. Further, the neutrophils remain metabolically active, capable of releasing cytokines, perform phagocytosis, and migrate in response to IL-8. Taken together, this data provides evidence of the potential efficacy of utilizing fostamatinib in bacterial sepsis.

Keywords

Sepsis; Spleen tyrosine kinase; Neutrophils

1. Introduction

Sepsis, defined as life-threatening organ dysfunction caused by a dysregulated host response to infection, leads to significant morbidity and mortality worldwide [1,2]. The innate immune response to sepsis involves neutrophils, which are the most abundant leukocyte in circulation and comprise the first line of defense against invading bacterial pathogens. Neutrophils protect the host from bacterial infections through a variety of important end-effector functions including phagocytosis, degranulation, generation of reactive oxygen species (ROS) and release of neutrophil extracellular traps (NETs) [3,4]. Unfortunately, neutrophils can be a double-edged sword in sepsis. Though vital for effective bacterial clearance, when hyperactivated, aberrant end-effector functions can contribute to significant end-organ dysfunction [5]. Specifically, during systemic infection neutrophils become sequestered in capillaries, activate endothelium, and migrate into tissues. Once they have migrated, they release pro-inflammatory cytokines and proteolytic enzymes, ROS, and NETs, all of which can be detrimental to host tissue. Therefore, there is interest in targeting hyperactive neutrophil activation as a potential therapeutic strategy in bacterial sepsis [6].

Spleen tyrosine kinase (SYK) is an intracellular non-receptor kinase expressed in a variety of hematopoietic cells including neutrophils [7]. Fostamatinib is an FDA-approved SYK inhibitor used for the treatment of chronic immune thrombocytopenia. We recently demonstrated that R406, the *in vitro* active component of fostamatinib, can inhibit the release of NETs when healthy donor neutrophils are stimulated with plasma from patients with coronavirus disease 2019 (COVID-19) [8]. Additionally, using samples from a phase II randomized clinical trial evaluating the safety of fostamatinib in COVID-19, we demonstrated that fostamatinib was associated with downregulation of hyperactivated neutrophils [9,10]. SYK signaling has been demonstrated to contribute to many multiple

neutrophil end-effector functions following lipopolysaccharide (LPS) stimulation [11–14]. Therefore, we aimed to determine if fostamatinib can modulate neutrophil activation and end-effector functions following LPS stimulation. We observed that R406 effectively regulates hyperactive neutrophil functions by inhibiting degranulation, the release of NETs, ROS production, and endothelial cell adherence in response to LPS stimulation, while preserving phagocytosis, migration, and cytokine release *in vitro*.

2. Methods

2.1. Human neutrophil isolation and stimulation

Whole blood was obtained from healthy donors (protocol number 17-CC-0148). Neutrophils were isolated within thirty minutes of blood draw using the EasySep Direct Human Neutrophil Isolation Kit (Stemcel, cat# 19666) following manufacturer instructions. Cells were quantified using TC-20 Cell Counter (Biorad, cat# 1450102) and resuspended in Gibco Opti-MEM Serum Reduced Media (ThermoFisher, cat# 31985070) containing 50 μg/mL of streptomycin and 50 mU/mL of penicillin (ThermoFisher, cat# 10378016). Neutrophils were stimulated with varying concentrations of LPS from *Klebsiella pneumoniae* (Millipore Sigma, cat# L4268), *Pseudomonas aeruginosa* 10 (Millipore Sigma, cat# L9143), or *Escherichia Coli* 5 (Invivogen, cat# tlrl-pb5lps) based on individual experiments. When inhibitors were added, cells were preincubated for thirty minutes prior to stimulation unless noted otherwise. R406 (the *in vitro* active component of fostamatinib) was used at a concentration of 1 μM (provided by Rigel Pharmaceuticals).

2.2. Live cell imaging of neutrophil extracellular traps

NETs were quantified using live cell imaging with an Incucyte S3 (Essen Bioscience). Neutrophils in media were mixed with 250 nM Cytotox Green Dye (Sartorius, cat# 4633) and Incucyte Nuclight Rapid Red Dye (Sartorius, cat# 4717) at a final concentration of 1:1000 in a 96-well plate. Cells were preincubated with 1 μM R406 and then stimulated with LPS from *Klebsiella pneumoniae*, *Pseudomonas aeruginosa,* or *Escherichia Coli* for 8 h. Neutrophils were imaged every 15 min with the phase, green laser (set for 150 ns absorbance) and the red laser (300 ns absorbance), acquiring 3 images per cell. Data was analyzed on the Incucyte S3 2022vC software. Briefly, red object segmentation was used to determine the number of cells per well. This analysis was performed using the surface fit program, with a threshold of object detection set at 0.6 Red Calibrated Units (RCUs), a pixel size of −2 (units), and edge sensitivity set to −25 (units) to differentiate between cells. A minimum area of 20 μMs and a maximum area of 300 μMs was set to avoid background detection. Neutrophils undergoing NETosis were identified similar to the surface fit program, setting a threshold of 1 green calibrated unit (GCU), a pixel size of −1, edge sensitivity turned off, and area filters between 100 μMs and 1250 μMs. Total neutrophil count per well was determined by the maximum red objects over 8 h. Data represents the percentage of neutrophils undergoing NETosis at any time point relative to the neutrophil count in each well. Data was collated from 5 independent experiments and neutrophil donors. A similar assay and settings have been previously utilized to quantify NETosis previously [15].

2.3. Detection of neutrophil extracellular trap formation by flow cytometry

For immunofluorescence studies, neutrophils suspended in RPMI1640 medium supplemented with 10 % FBS were dispensed into 1.5 ml microcentrifuge tubes per condition and stimulated with 5 μg/ml LPS isolated from *Klebsiella pneumoniae* (Millipore Sigma, cat# L4268) for 1 h at 37 °C and 5 % CO_2. At the end of incubation, neutrophils were stained with 200 nM SYTOX Green (Invitrogen™, cat# S7020) for 10 min at 37 °C. Cells were washed with FACS buffer (Rockland, cat# MB-086–0500) and fixed with 4 % formalin (final concentration of 1 %). Following centrifugation at 800xg for 8 min, pelleted cells were treated with Fc receptor blocking solution (BioLegend, Human TruStain FcX™, cat#422301) for 30 min. Cells were incubated with primary antibodies, APC anti-human myeloperoxidase (MPO) (130–129–211; Miltenyi Biotech, cat#130–129–211) and Rabbit anti-Histone H3 (citrulline R2 + R8 + R17) (abcam, cat# ab5103) in FACS buffer containing Fc block for 1 h at 4 °C. Cells were washed with FACS buffer and resuspended in secondary antibody AlexaFluor 594 Donkey F(ab')2 anti-Rabbit IgG (abcam, cat #ab150072;) for 45 min. After washing in FACS buffer, cells were acquired in an LSRFortessa™ (BD Biosciences) flow cytometer. Data were analyzed from 6 individual neutrophil donors by FlowJo 10.10.0 software.

2.4. Indirect measurement of reactive oxygen species and metabolism

Neutrophils were resuspended in XF RPMI Medium, pH 7.4 (Agilent, cat# 103576–100) supplemented with 2 mM L-glutamine (Agilent, cat# 103579–100), 1 mM sodium pyruvate (Agilent, cat# 103578–100), and 10 mM glucose (Agilent, cat# 103577–100). Neutrophils were adhered to a Cell-Tak (Corning, cat# 354240) coated cell culture microplate (Agilent, cat# 102601–100) for 30 min at room temperature without CO_2. Diphenyleneiodonium chloride (DPI) (Fisher, Cat# AC328660250), LPS (*Klebsiella pneumoniae* or *Pseudomonas aeruginosa)* and R406 injections were prepared in non-supplemented XF RPMI media and loaded into the ports of the sensor cartridge (Agilent, cat# 102601–100). During instrument calibration (Agilent, Seahorse XFe96 Extracellular Analyzer, Linthicum, MD), neutrophils were counted on a Biotek Cytation 1 Imaging Reader (Agilent, Linthicum, MD). Following the initiation of measurements, the oxygen consumption rate (OCR) and extracellular acidification rate (ECAR) were measured every 5.5 min for approximately 230 min. Data were normalized according to cell counts and exported from the Wave Desktop software (Agilent, Wave Desktop 2.6, Version 2.6.1) for downstream analyses. To minimize batch-to-batch variation, normalization of the data was performed by calculating the average maximum peak height for the LPS condition across all technical replicates. The data presented represents the area under the curve (AUC) over the course of the experiment or the peak rate across 4 independent experiments and neutrophil donors.

2.5. Direct measurement of reactive oxygen species

Neutrophils were plated in 100 μL of media as previously described. Cells were preincubated with R406 for 30 min prior to stimulation with LPS from *Klebsiella pneumoniae*, *Pseudomonas aeruginosa,* or *Escherichia Coli*. Luminol (Millipore-Sigma, cat# A8511) or isoluminol (Millipore-Sigma, cat# A8264) was added simultaneously to LPS to the wells, at a final concentration of 60 μM or 10 μM respectively. Luminol detects total

ROS (intracellular and extracellular), while isoluminol detects only extracellular ROS due to its inability to cross the cellular membrane. Cells were incubated at 37 °C for two hours in a Victor Nivo Multimode Plate Reader (PerkinElmer). Chemiluminescence was measured every 5 min, reading each well for 500 ms. Emission was normalized to zero at experiment start for each well, and for kinetic graphs raw data was fit with a zeroeth order smoothing polynomial utilizing an average of 2 neighbors. All data represents the AUC of emission over the course of the experiment or peak emission across 5 independent experiments and donors.

2.6. Measurement of degranulation and cytokine release

Neutrophils were plated in 100 μL of media and preincubated with 1 μM R406 and subsequently exposed to LPS from *Klebsiella pneumoniae*. Following one hour of stimulation, cells were spun at 336 xg, cell adherence to the plate was verified by microscopy, and supernatants were extracted and frozen at −80 °C. Quantification of cytokine, chemokines and degranulation markers from cell supernatants was performed using the ProcartaPlex 15 plex Luminex assay (ThermoFisher). The analytes of interest were MCP-1 (CCL2), MIP-1 alpha (CCL3), MIP-2 alpha (CXCL2), MMP-9, Myeloperoxidase (MPO), NGAL, S100A8/A9, TNF-α, GRO alpha (KC/CXCL1), IL-1β, IL-6, IL-10, IP-10 (CXCL10), Arginase-1, and Lactoferrin. Informative biomarkers were included in the analysis. Technical issues prevented measurement of MIP-1 alpha (CCL3), MIP-2 alpha (CXCL2), CXCL-1, Arginase-1, and S100A8/A9 across all samples and thus they were removed from all analyses. Standard curves were computed for each analyte using Bio-Rad Bioplex software. Analyte values were averaged across technical replicates, log-transformed, and the average concentration of each analyte was compared across 5 independent experiments and donors.

2.7. Measurement of surface makers of neutrophil activation

Neutrophils were plated in 100 μL of media, preincubated with 1 μM R406 and stimulated with LPS from *Klebsiella pneumoniae* for 1 h. Cells were spun at 336 xg for 5 min and the supernatant was removed. Cells were resuspended in FACS buffer (PBS+2% FBS) with 10 μL of human Fc Blocking Reagent (Miltenyi Biotec, cat# 130–059–901) in a total volume of 100 μL. Cells were incubated on ice for 10 min. Following blocking, cells were spun as described previously. Subsequently, cells were resuspended in 100ul of FACS buffer containing antibodies to CD11b (ICRF44, Biolegend), CD64 (10.1, Biolegend), CD16 (3G8, BD), CD62L (DREG-56, BD) and incubated on ice for 30 min. Following staining, cells were spun and washed with 200 μL of FACS buffer and fixed in 4 % PFA (FD Neurotechnologies Incorporated, cat# PF101) for 15 min on ice. Following fixation, cells were washed and spun at 336 xg for 5 min, resuspended in 100 μL of FACS buffer, and acquired in a BD FACSymphony A5 flow cytometer, Data were analyzed using Flowjo version 10.9. Gates were drawn based on Fluorescence Minus One (FMO) control's run on each experiment. Average Mean Fluorescent Intensities (MFI's) or percentages of cell types were computed across technical replicates, and data was collated across 5 independent experiments and donors.

2.8. Imaging cytometry of cell circularity

Neutrophils were incubated in a 1.5 mL Eppendorf tube with 1 mL of media. Cells were preincubated with 1 μM R406 for 30 min and stimulated with LPS from *Klebsiella pneumoniae* for 1 h. Following incubation, cells were spun down at 336 xg for 5 min and supernatant was removed. 250 μL of Cytofix/Cytoperm (BD, cat# 554714) was added to each tube, and cells were incubated on ice for 15 min. Following fixation and permeabilization, cells were spun at 336 xg and washed with 1 mL of Permwash buffer (BD, cat# 554723). Cells were spun and resuspended in a total volume of 100 μL of Permwash and Fc Blocker (Miltenyi Biotec, cat# 130–059–901). Cells were incubated on ice for 20 min. Following blocking, cells were spun and resuspended in 100 μL 1X permwash. Cells were incubated on ice for 30 min. Following incubation, cells were washed with 1 mL of 1X permwash, spun, and subsequently fixed in 1 % PFA (FD Neurotechnologies Incorporated, cat# PF101) for 20 min on ice. Cells were washed and spun at 336xg and resuspended in 40 μL of PBS. Data was acquired on an Amnis Imagestream MarkII and analyzed using IDEAs software. Circular cells were defined as having a circularity score > 10 based on manufacturer's recommendations and averaged across technical replicates. Data represents collated results from n = 3 donors.

2.9. Phagocytosis of E. coli and S. aureus bioparticles

Neutrophils were plated in 100 μL of media. Incucyte Nuclight Rapid Red Dye (Sartorius, cat# 4717) was added at a final concentration of 1:1000. Cells were preincubated with 1 μM R406 or 10 μg/mL of Cytochalasin D (ThermoFisher, cat# PHZ1063) for 30 min. After preincubation, 1 μg of pHrodo® Green *E. coli* Bioparticles® for Incucyte® (Sartorius, cat# 4616) or 1 μg of pHrodo® Green *Staphylococcus aureus* Bioparticles® for Incucyte® (Sartorius, cat# 4619) were added to all wells. Cells are then incubated for 8 h in the Incucyte S3, imaged every 15 min with the green laser (set for 150 ns absorbance) and the red laser (300 ns), acquiring 3 images per cell at each time point. Subsequent analysis was then performed using the Incucyte S3 2022vC software. Number of neutrophils per well was determined through identical analysis as performed for NETosis experiments. Number of phagocytic neutrophils were determined through green surface fit segmentation on the Incucyte S3 2022vC basic analysis, with Edge split turned on and set at zero. Pixel size was set at 0, and area filters between 10 and 1000 μM used to avoid background. Number of phagocytic neutrophils at time-zero was set to zero, and the increase in phagocytic neutrophils was measured over 8 h. Number of phagocytosing neutrophils were normalized to total cell count per well. Data was averaged across technical replicates and represents collated results from 5 independent experiments and donors.

2.10. Cellular migration

Neutrophils were plated in 100 uL of media in Corning Transwell cell culture insert (Millipore-Sigma, cat# CLS3415). Cells were preincubated with 1 μM R406 for 30 min. After preincubation, 10 ng/mL of E. coli LPS (EB Ultrapure Invivogen, cat# tlrl-pb5lps) was added to selected wells. In the exterior compartment, 1 mL of Gibco Opti-MEM with 10 nM of human recombinant IL-8 (Bio-techne R&D, cat# P10145.1) was added and neutrophils were allowed to incubate for 1 h. Following a one-hour migration, the internal compartments

of Transwell cell plates were removed and plates were placed in Incucyte S3 with nine phase images taken per well. Following imaging, the cell-by-cell function on the Incucyte 2022vC was used to compute the number neutrophils present in each well with the Cell Boundary Segmentation Adjustment set at 0.1 and Seed settings set at a cell contrast of 2 and a cell morphology of 2. Finally, the cell-by-cell settings included a minimum cellular area of 75 μM^2, and a maximum area of 1500 μM^2. The total number of neutrophils was summed across the nine images per well, and the results were averaged across technical replicates. Data represents collated results of 5 independent experiments and donors.

2.11. Cellular adhesion

Human Umbilical Vein Endothelial Cells (HUVECs; Lonza#C2519A), were cultured in EGM™−2 Endothelial Cell Growth Medium-2 (Lonza# CC-3162). Forty-eight hours prior to each experiment, 96-well tissue culture plates (Corning#3603) were coated with gelatin (0.2 %; Sigma#G1393–100ML), washed and air dried for 2 h. HUVECs at passage five to six were then seeded onto the gelatin precoated 96-well plates and allowed to grow in EGM™−2 for 48 h. On the day of experiment, the medium was replaced with Opti-MEM™ I Reduced Serum Medium (ThermoFishe#31985070) and HUVECs were incubated 3–4 h until neutrophils were added. Neutrophils at a concentration of 1 million cells per mL were labeled with 2.5 μM CellTracker Green CMFDA (5-chloromethylfluorescein diacetate; Thermo Fisher Scientific#C7025) fluorescent dye in Hanks' Balanced Salt Solution (HBSS; Thermo Fisher Scientific # 14175–095) for 15 min at room temperature. Thereafter, CMFDA dye was washed off and resuspended at 1million per 4 mL in Opti-MEM. Neutrophils were subsequently stimulated with LPS from *Klebsiella pneumoniae* for one hour either with or without R406 pretreatment in a 37 °C incubator with 5 % CO_2. Media was removed and 200 μL of neutrophils exposed to different treatment conditions were added to HUVECs at a concentration of 50,000 cells per well and incubated for 30-minute in a 37 °C incubator with 5 % CO_2. After incubation, neutrophils were gently aspirated out and wells were washed once with 150 μL of HBSS. HBSS was subsequently removed, and cells were fixed for at least 1 h by adding 100 μl per well 4 % paraformaldehyde (PFA; Thermo Fisher Scientific #J61899.AP). Neutrophil adhesion to HUVECs were captured using Cytation 5 Cell Imaging Multi-Mode Reader (BioTek) configured with a GFP imaging filter cube and a 10X objective controlled by Gen5 microplate reader and imager software. The number of adherent neutrophils per well in the captured images were determined using Gen5 microplate reader and imager software' Cellular Analysis Cell Count tool. For counting, threshold for fluorescence was set at 30,000 RU, and object size was set between 10 and 30 μm. Data represents collated results of 5 independent experiments and donors.

2.12. Statistical analysis

To compare between non stimulated, LPS stimulated, and LPS stimulated cells + R406, a repeated measure one-way ANOVA with Geiser-Greenhouse correction was utilized to measure overall significant differences between the groups. Further multiple comparisons were utilized to measure differences between all groups, utilizing Tukey correction to correct for multiple comparisons. All statistics performed in GraphPad Prism (Prism 10 for macOS, Version 10.1.0) Stars represent results of multiple comparisons. $p < 0.05$*, $p < 0.01$**, $p < 0.001$***, $p < 0.0001$****.

3. Results

3.1. R406 inhibits gram-negative bacterial LPS Induced NETosis

Based on our COVID-19 findings, we initially sought to determine if R406 can prevent LPS-induced NETosis. Neutrophil stimulation with K. *pneumoniae* LPS led to a nearly three-fold increase in NETosis eight hours post-stimulation compared with non-stimulated cells, a finding prevented by R406 preincubation (Fig. 1A). R406-mediated NET inhibition began 2 h post-LPS stimulation and increased over time (Fig. 1B). This effect was not limited to K. *pneumoniae*, as R406 had a similar effect on neutrophils stimulated with LPS isolated from P. *aeruginosa* and E. *coli* (Fig. S1A–F.) Further, we confirmed our finding that K. *pneumoniae* LPS-induced NETosis is inhibited by R406 with a flow cytometry assay that directly detects NETs co-expression of extracellular DNA, MPO, and tricitrullinated histones (Figure S2 and S3).

3.2. R406 inhibits gram-negative bacterial LPS-induced neutrophil ROS generation

Because LPS induced NETosis has been shown to be ROS-dependent [16], we characterized neutrophil ROS generation following LPS stimulation with and without R406 treatment. First, we quantified neutrophil oxygen consumption rate (OCR) as a surrogate marker for ROS production. OCR peaked 15 to 20 min post K. *pneumoniae* LPS stimulation (Fig. 1C). Pre-treatment with R406 significantly decreased the total and peak OCR over one hour as well as the maximum OCR following LPS stimulation (Fig. 1D and Fig. S4A). R406 had a similar impact on *P. aeruginosa* stimulated neutrophils (Fig. S4B, S4C). Subsequently, we aimed to directly assess whether R406 could diminish both total ROS (intracellular and extracellular) and ROS secreted by neutrophils (extracellular alone). We directly quantified total (i.e., intra- and extracellular) ROS by luminol-based chemiluminescent assay and extracellular ROS alone by an isoluminol-based assay. Total ROS and extracellular ROS alone significantly increased post *K. pneumoniae* LPS stimulation, which was prevented by preincubation with R406 (Fig. 1E–G and Fig S5A–C). R406 preincubation also prevented the generation of both total ROS and extracellular ROS following *P. aeruginosa* or *E. coli* LPS stimulation (Figure S6A–D and Figure S7A–D). In experiments designed to determine if delayed R406 administration might be beneficial, we observed R406 significantly decreased neutrophil total and peak OCR when added 10 min following *K. pneumoniae or P. aeruginosa* stimulation (Fig. 1H and I, Figure S8A–C).

3.3. R406 significantly reduces degranulation, while having minimal impact on cytokine release

Following *K. pneumoniae* LPS stimulation for one hour we observed a significant increase in soluble levels of MPO and trends towards increased lactoferrin and MMP-9 (Fig. 2A and Table S1). In neutrophils preincubated with R406 we observed a significant reduction in cell culture supernatant levels of MPO post *K. pneumoniae* LPS stimulation. Evaluating cytokines we found significant increases in neutrophil supernatant levels of TNF-α, IL-6, and IL-1β at one hour post *K. pneumoniae* LPS stimulation, which were not significantly reduced by R406 preincubation (Fig. 2B and Table S1). Interestingly, statistically significant increases in CXCL10 were inhibited by R406.

3.4. R406 has minimal impact on LPS-induced upregulation of neutrophil surface markers of activation

Next, we sought to analyze neutrophil surface markers commonly observed in bacterial sepsis following LPS stimulation. LPS stimulation led to significant reduction in CD62L and increases in CD11b and CD64 expression (Fig. 3A–C, Table S3). We observed that R406 did not inhibit LPS-induced reduction in CD62L surface expression (Fig. 3A). Similarly, R406 did not inhibit CD11b or CD64 upregulation (Fig. 3B–C). Following LPS stimulation, we saw a population of $CD16^{low}$ neutrophils emerge that was not present in non-stimulated cells (Fig. 3D–E). Interestingly, pre-incubation with R406 reversed this trend, significantly reducing the percentage of $CD16^{low}$ neutrophils (Fig. 3D–3E).

3.5. R406 increases cell migration but inhibits endothelial cell adhesion

To assess migration, we used a Transwell assay to quantify the ability of neutrophils to migrate in response to IL-8. When exposed to E. *coli* LPS, we observed no change in the number of neutrophils migrating in response to IL-8, however, when exposed to R406, we observed a 10-fold increase in the number of migrating neutrophils in response to IL-8 in the presence or absence of *E. coli* LPS (Fig. 4A and Figure S9A).

We next evaluated the impact of R406 on the ability of neutrophils to adhere to HUVECs. First, we found that stimulation with K. *pneumoniae* LPS significantly increased the number of cells adhering to HUVEC cells (Figure S9B). Interestingly, R406 preincubation was able to significantly reduce in the number of adherent neutrophils following 30 min of co-culture (Fig. 4B, Figure S9C–D).

Seeing changes in endothelial adhesion, we wanted to further investigate the effects of R406 on neutrophil shape and morphology using high throughput imaging flow cytometry. K. *pneumoniae* stimulated neutrophils demonstrated a variety of non-circular phenotypes not seen in non-stimulated circular neutrophils (Figure S10A–B). Stimulation with K. *pneumoniae* LPS significantly increased the proportion of non-circular neutrophils, while preincubation with R406 significantly abrogated this LPS-induced phenotype (Fig. 4C, Figure S10C–E).

3.6. R406 does not impact phagocytosis but does decrease overall cellular metabolism

We next determined whether R406 impacts phagocytosis, a vital host defense mechanism. Neutrophils were incubated with E. *coli* and S. *aureus* bioparticles and phagocytosis was quantified by live cell imaging. Preincubation with R406 had no significant effect on phagocytosis for either bioparticle, while Cytochalasin D, an inhibitor of actin polymerization and thus phagocytosis, did significantly reduce bioparticle phagocytosis (Fig. 4D–E, Figure S11A–C).

After observing decreases in NETosis and ROS generation, but minimal changes in phagocytosis and cytokine release, we aimed to gain a wider view of overall cellular metabolic activity by measuring extracellular acidification rate (ECAR) an indicator of glycolysis. We found that ECAR increased following LPS stimulation and peaked within 10 min, which was significantly reduced with R406 (Fig. 4F–G). It is important to note

that while the R406-treated neutrophils had lower ECAR than LPS alone, they still had significantly higher rates of ECAR than non-stimulated cells alone (Fig. 4G). Furthermore, R406 treatment 10 min post-stimulation reduced the metabolic increases following *K. pneumoniae* LPS stimulation (Fig. 4H–I). These trends were consistent across multiple LPS species, as we same similar trends in *P. aeruginosa* stimulated neutrophils (Figure S12A–B).

4. Discussion

While neutrophils are protective against invading bacterial pathogens, many clinical outcomes and ultimately mortality in sepsis have been associated with a pathogenic overactivation of neutrophils [17]. Through a series of functional and cellular assays we demonstrate that treatment with R406 impacts many end-effector functions of neutrophils thought to contribute to pathogenesis in sepsis, demonstrating its potential efficacy as a regulator of neutrophil activation in the setting of LPS stimulation. Specifically, we demonstrate that R406 mitigates neutrophil NETs release, ROS generation, degranulation, and binding to endothelium. Despite inhibition of these end-effector functions other key functions remain intact including migration, phagocytosis, and inflammatory cytokine release. Most findings were consistent across LPS from *K. pneumoniae, P. aeruginosa*, and *E. coli* when tested. These findings suggest potential utility of targeting SYK to modulate pathogenic neutrophil responses during bacterial sepsis.

High levels of NETs correlate with disease severity in sepsis and have been demonstrated to be predictive of worse outcomes [18]. During infection, NETs are thought to be protective by inhibiting the dissemination of invading pathogens. However, NETs contribute to sepsis pathogenesis because they are pro-coagulant and activate endothelium [5]. Our data show that R406 can abrogate LPS-induced NETosis *in vitro,* highlighting the potential for R406 to decrease NET-mediated coagulopathy, endothelial cell activation, and organ damage *in vivo*.

Circulating markers of neutrophil degranulation and ROS generation are associated with increased sepsis severity and mortality [19–21]. We show that R406 inhibits LPS-induced neutrophil myeloperoxidase release *in vitro* and demonstrate by direct and indirect assays that R406 effectively decreases intra and extracellular ROS generation when administered prophylactically or therapeutically (i.e., before or after LPS-stimulation, respectively). These findings provide biologic plausibility that R406 mediated inhibition of NETosis, which is dependent on intracellular ROS generation, and extracellular release of ROS, which is associated with oxidized lipids and proteins that induce cellular injury and end-organ dysfunction, might provide therapeutic benefit in bacterial sepsis [16,22,23].

During sepsis activated neutrophils adhere to endothelium contributing to microvascular dysfunction or transmigrate into tissues contributing to pathogen clearance and tissue injury [24–26]. We demonstrate that R406 decreases neutrophil adhesion to endothelial cells and increases migration towards IL-8 *in vitro*. This data is similar to prior reports that have demonstrated that adhesion of neutrophils is inhibited in murine SYK-knockout neutrophils, but cellular migration is not impacted [12]. Finally, these findings are further supported by our imaging flow cytometry analysis, as decreases in cellular circularity have been found to correlate with mobility and activation in complement-stimulated neutrophils, a phenotype

we were able to ameliorate with R406 pretreatment [27]. Our findings provide a therapeutic approach in which R406 decreases neutrophil adhesion to endothelial cells, potentially mitigating neutrophil-mediated endothelial cell activation and microvascular dysfunction, while maintaining the ability to migrate.

Ex vivo studies of SYK-knockout murine neutrophils stimulated with serum opsonized *Staphylococcus aureus* and *E. coli* have observed decreased granule release, NETosis, reactive oxygen species, while other functions remain intact such as the release of inflammatory cytokines, including IL-6 and IL-1β, and *E. coli* phagocytosis. These findings are consistent with our work. However, there are differences in findings from the SYK-knockout neutrophils and our study with SYK inhibition of human neutrophils with R406, such as the impact on CD11b activation and loss of CD62L and phagocytosis on *Staphylococcus aureus*. These disparate findings can likely be explained by continued expression of SYK while altering SYK phosphorylation in R406 treated neutrophils instead of knockout kinetics in the mouse neutrophils, differences in neutrophil end effector function in mouse versus primary human neutrophils, and different responses based on stimuli used. Further, R406 has been shown to effectively inhibit SYK phosphorylation as well as inhibit a variety of other kinases and thus could be having effects on additional non-SYK mediated pathways [28].

R406 has been shown to mitigate end-organ dysfunction and myeloid activation in LPS mouse models of acute kidney injury and acute lung injury and a cecal ligation and puncture model of sepsis [29–31]. However, *in vivo* models of SYK-knockout neutrophils result in a reduction in bacterial clearance in the absence of antibiotics [32]. Future studies to evaluate the impact of SYK inhibition, and specifically R406 treatment, in combination with antibiotics will be important.

Classically, LPS activates TLR4 in innate immune cells, which subsequently signals through either a MyD88 dependent cellular surface pathway or a TRIM/TRAF intracellular pathway. The exact role of SYK in this pathway is unclear and debated in the literature. SYK conventionally binds to immune-receptor tyrosine-based activation motif (ITAMs) on receptors such as Fcγ receptors, c-type lectin receptors, and integrins [33]. TLR4 contains a hem-ITAM, and multiple studies have shown co-immunoprecipitation of TLR4 and SYK in a variety of innate immune cells, suggesting that SYK may be directly phosphorylated by TLR4 [14]. Evidence from neutrophils suggests that LPS stimulation leads to SYK phosphorylation and the formation of a TLR4, p-SYK, p-CEACAM1 complex, which results in ROS production and IL-1β release [11]. Other studies have demonstrated SYK as being vital to endosomal uptake of TLR4 through a number of potential linker molecules such as CD14, DAP12, SCIMP, and TREM1. Thus, SYK inhibition could modulate the downstream signaling pathways impacted by TLR4 endocytosis in the context of LPS stimulation [34–36]. Our experiment does not offer a definitive explanation of the underlying mechanism by which R406 is able to inhibit various neutrophil functions in the context of LPS stimulation, therefore further studies are needed to elucidate these mechanistic pathways.

Limitations of our study are that these are *in vitro* studies and *in vivo* studies are needed to confirm these findings. However, many of our findings have been recapitulated using *in*

vitro mouse models and *in vivo* small animal models. Further, the effects of purified LPS represent an incomplete picture of how whole live bacteria or other pathogen associated molecular patterns (PAMPs) derived from gram-negative bacteria interact with neutrophils during sepsis and how these interactions may be impacted by R406. Additionally, we did not test the efficacy of R406 on modulating neutrophil responses in the context of gram-positive bacteria. Lastly, neutrophil responses to LPS are broadly impacted by other cell types, with studies suggesting platelets are vital to efficient NETosis in the context of low levels of LPS for example [37,38]. Thus, it is important to test the effects of R406 following LPS stimulation of other cell types *in-vitro*, co-culture assays, and using gram positive bacteria.

Our findings highlight R406 as a promising novel therapeutic mechanism in bacterial sepsis, offering a strategy to temper the excessive neutrophil responses without compromising their critical roles in host defense. Taken together our *in vitro* data and the results of small animal models provide a strong rationale for evaluating the efficacy of fostamatinib in large animal models of bacterial sepsis and evaluating the trajectory of SYK expression during human bacterial sepsis.

Supplementary Material

Refer to Web version on PubMed Central for supplementary material.

Funding

This work has been funded in part by the Intramural Research Program of the National Institutes of Health Clinical Center, the Division of Intramural Research, National Institute of Allergy and Infectious Diseases (NIAID), and the Intramural program of the National Heart Lung and Blood Institute (ZIAHL006267, ZIAHL006262, ZIAHL006263).

Data availability

Data will be made available on request.

References

[1]. Rhee C, Dantes R, Epstein L, Murphy DJ, Seymour CW, Iwashyna TJ, Kadri SS, Angus DC, Danner RL, Fiore AE, et al. , Incidence and trends of sepsis in US hospitals using clinical vs claims data, 2009–2014, J. Am. Med. Assoc. 318 (13) (2017) 1241–1249.

[2]. Kadri SS, Rhee C, Strich JR, Morales MK, Hohmann S, Menchaca J, Suffredini AF, Danner RL, Klompas M, Estimating ten-year trends in septic shock incidence and mortality in United States academic medical centers using clinical data, Chest 151 (2) (2017) 278–285. [PubMed: 27452768]

[3]. Zhang F, Liu AL, Gao S, Ma S, Guo SB, Neutrophil dysfunction in sepsis, Chin. Med. J. (Engl) 129 (22) (2016) 2741–2744. [PubMed: 27824008]

[4]. Kovach MA, Standiford TJ, The function of neutrophils in sepsis, Curr. Opin. Infect. Dis. 25 (3) (2012) 321–327. [PubMed: 22421753]

[5]. Denning NL, Aziz M, Gurien SD, Wang P, DAMPs and NETs in sepsis, Front. Immunol. 10 (2019) 2536. [PubMed: 31736963]

[6]. Shen X, Cao K, Zhao Y, Du J, Targeting neutrophils in sepsis: from mechanism to translation, Front. Pharmacol. 12 (2021) 644270.

[7]. Braselmann S, Taylor V, Zhao H, Wang S, Sylvain C, Baluom M, Qu K, Herlaar E, Lau A, Young C, et al. , R406, an orally available spleen tyrosine kinase inhibitor blocks fc receptor signaling

and reduces immune complex-mediated inflammation, J. Pharmacol. Exp. Ther. 319 (3) (2006) 998–1008. [PubMed: 16946104]

[8]. Strich JR, Ramos-Benitez MJ, Randazzo D, Stein SR, Babyak A, Davey RT, Suffredini AF, Childs RW, Chertow DS, Fostamatinib inhibits neutrophils extracellular traps induced by COVID-19 patient plasma: a potential therapeutic, J. Infect Dis. 223 (6) (2021) 981–984. [PubMed: 33367731]

[9]. Wigerblad G, Warner SA, Ramos-Benitez MJ, Kardava L, Tian X, Miao R, Reger R, Chakraborty M, Wong S, Kanthi Y, et al. , Spleen tyrosine kinase inhibition restores myeloid homeostasis in COVID-19, Sci. Adv. 9 (1) (2023) eade8272.

[10]. Strich JR, Tian X, Samour M, King CS, Shlobin O, Reger R, Cohen J, Ahmad K, Brown AW, Khangoora V, et al. , Fostamatinib for the treatment of hospitalized adults with coronavirus disease 2019: a randomized trial, Clin. Infect. Dis. 75 (1) (2022) e491–e498. [PubMed: 34467402]

[11]. Lu R, Pan H, Shively JE, CEACAM1 negatively regulates IL-1beta production in LPS activated neutrophils by recruiting SHP-1 to a SYK-TLR4-CEACAM1 complex, PLoS Pathog. 8 (4) (2012) e1002597.

[12]. Mocsai A, Zhou M, Meng F, Tybulewicz VL, Lowell CA, Syk is required for integrin signaling in neutrophils, Immunity 16 (4) (2002) 547–558. [PubMed: 11970878]

[13]. Arndt PG, Suzuki N, Avdi NJ, Malcolm KC, Worthen GS, Lipopolysaccharide-induced c-Jun NH2-terminal kinase activation in human neutrophils: role of phosphatidylinositol 3-Kinase and Syk-mediated pathways, J. Biol. Chem. 279 (12) (2004) 10883–10891. [PubMed: 14699155]

[14]. Miller YI, Choi SH, Wiesner P, Bae YS, The SYK side of TLR4: signalling mechanisms in response to LPS and minimally oxidized LDL, Br. J. Pharmacol. 167 (5) (2012) 990–999. [PubMed: 22776094]

[15]. Gupta S, Chan DW, Zaal KJ, Kaplan MJ, A high-throughput real-time imaging technique to quantify NETosis and distinguish mechanisms of cell death in human neutrophils, J. Immunol. 200 (2) (2018) 869–879. [PubMed: 29196457]

[16]. Azzouz D, Khan MA, Palaniyar N, ROS induces NETosis by oxidizing DNA and initiating DNA repair, Cell Death Discov. 7 (1) (2021) 113. [PubMed: 34001856]

[17]. Shen XF, Cao K, Jiang JP, Guan WX, Du JF, Neutrophil dysregulation during sepsis: an overview and update, J. Cell Mol. Med. 21 (9) (2017) 1687–1697. [PubMed: 28244690]

[18]. Maruchi Y, Tsuda M, Mori H, Takenaka N, Gocho T, Huq MA, Takeyama N, Plasma myeloperoxidase-conjugated DNA level predicts outcomes and organ dysfunction in patients with septic shock, Crit. Care 22 (1) (2018) 176. [PubMed: 30005596]

[19]. Schrijver IT, Kemperman H, Roest M, Kesecioglu J, de Lange DW, Myeloperoxidase can differentiate between sepsis and non-infectious SIRS and predicts mortality in intensive care patients with SIRS, Intensive Care Med. Exp. 5 (1) (2017) 43. [PubMed: 28916973]

[20]. Lu J, Liu J, Li A, Roles of neutrophil reactive oxygen species (ROS) generation in organ function impairment in sepsis, J. Zhejiang Univ. Sci. B 23 (6) (2022) 437–450. [PubMed: 35686524]

[21]. Wang M, Zhang Q, Zhao X, Dong G, Li C, Diagnostic and prognostic value of neutrophil gelatinase-associated lipocalin, matrix metalloproteinase-9, and tissue inhibitor of matrix metalloproteinases-1 for sepsis in the emergency department: an observational study, Crit. Care 18 (6) (2014) 634. [PubMed: 25407832]

[22]. Khan MA, Farahvash A, Douda DN, Licht JC, Grasemann H, Sweezey N, Palaniyar N, JNK activation turns on LPS- and Gram-negative bacteria-induced NADPH oxidase-dependent suicidal NETosis, Sci. Rep. 7 (1) (2017) 3409. [PubMed: 28611461]

[23]. Vorobjeva N, Prikhodko A, Galkin I, Pletjushkina O, Zinovkin R, Sud'ina G, Chernyak B, Pinegin B, Mitochondrial reactive oxygen species are involved in chemoattractant-induced oxidative burst and degranulation of human neutrophils in vitro, Eur. J. Cell Biol. 96 (3) (2017) 254–265. [PubMed: 28325500]

[24]. Park I, Kim M, Choe K, Song E, Seo H, Hwang Y, Ahn J, Lee SH, Lee JH, Jo YH, et al. , Neutrophils disturb pulmonary microcirculation in sepsis-induced acute lung injury, Eur. Respir. J. 53 (3) (2019).

[25]. Chishti AD, Shenton BK, Kirby JA, Baudouin SV, Neutrophil chemotaxis and receptor expression in clinical septic shock, Intensive Care Med. 30 (4) (2004) 605–611. [PubMed: 14991094]

[26]. Lerman YV, Kim M, Neutrophil migration under normal and sepsis conditions, Cardiovasc. Hematol. Disord. Drug Targets 15 (1) (2015) 19–28.

[27]. Denk S, Taylor RP, Wiegner R, Cook EM, Lindorfer MA, Pfeiffer K, Paschke S, Eiseler T, Weiss M, Barth E, et al. , Complement C5a-induced changes in neutrophil morphology during inflammation, Scand. J. Immunol. 86 (3) (2017) 143–155. [PubMed: 28671713]

[28]. Rolf MG, Curwen JO, Veldman-Jones M, Eberlein C, Wang J, Harmer A, Hellawell CJ, Braddock M, In vitro pharmacological profiling of R406 identifies molecular targets underlying the clinical effects of fostamatinib, Pharmacol. Res. Perspect. 3 (5) (2015) e00175.

[29]. Al-Harbi NO, Nadeem A, Ahmad SF, Alanazi MM, Aldossari AA, Alasmari F, Amelioration of sepsis-induced acute kidney injury through inhibition of inflammatory cytokines and oxidative stress in dendritic cells and neutrophils respectively in mice: Role of spleen tyrosine kinase signaling, Biochimie 158 (2019) 102–110. [PubMed: 30599182]

[30]. Nadeem A, Ahmad SF, Al-Harbi NO, Al-Harbi MM, Ibrahim KE, Kundu S, Attia SM, Alanazi WA, AlSharari SD, Inhibition of spleen tyrosine kinase signaling protects against acute lung injury through blockade of NADPH oxidase and IL-17A in neutrophils and gammadelta T cells respectively in mice, Int. Immunopharmacol. 68 (2019) 39–47. [PubMed: 30611000]

[31]. Issara-Amphorn J, Chancharoenthana W, Visitchanakun P, Leelahavanichkul A, Syk inhibitor attenuates polymicrobial sepsis in fcgriib-deficient lupus mouse model, the impact of lupus characteristics in sepsis, J. Innate Immun. 12 (6) (2020) 461–479. [PubMed: 32927460]

[32]. Van Ziffle JA, Lowell CA, Neutrophil-specific deletion of Syk kinase results in reduced host defense to bacterial infection, Blood 114 (23) (2009) 4871–4882. [PubMed: 19797524]

[33]. Mocsai A, Ruland J, Tybulewicz VL, The SYK tyrosine kinase: a crucial player in diverse biological functions, Nat. Rev. Immunol. 10 (6) (2010) 387–402. [PubMed: 20467426]

[34]. Ciesielska A, Matyjek M, Kwiatkowska K, TLR4 and CD14 trafficking and its influence on LPS-induced pro-inflammatory signaling, Cell. Mol. Life Sci. 78 (4) (2021) 1233–1261. [PubMed: 33057840]

[35]. Liu L, Lucas RM, Nanson JD, Li Y, Whitfield J, Curson JEB, Tuladhar N, Alexandrov K, Mobli M, Sweet MJ, et al. , The transmembrane adapter SCIMP recruits tyrosine kinase Syk to phosphorylate Toll-like receptors to mediate selective inflammatory outputs, J. Biol. Chem. 298 (5) (2022) 101857.

[36]. Dower K, Ellis DK, Saraf K, Jelinsky SA, Lin LL, Innate immune responses to TREM-1 activation: overlap, divergence, and positive and negative cross-talk with bacterial lipopolysaccharide, J. Immunol. 180 (5) (2008) 3520–3534. [PubMed: 18292579]

[37]. Liu S, Su X, Pan P, Zhang L, Hu Y, Tan H, Wu D, Liu B, Li H, Li H, et al. , Neutrophil extracellular traps are indirectly triggered by lipopolysaccharide and contribute to acute lung injury, Sci. Rep. 6 (2016) 37252. [PubMed: 27849031]

[38]. Demaret J, Venet F, Friggeri A, Cazalis MA, Plassais J, Jallades L, Malcus C, Poitevin-Later F, Textoris J, Lepape A, et al. , Marked alterations of neutrophil functions during sepsis-induced immunosuppression, J. Leukoc. Biol. 98 (6) (2015) 1081–1090. [PubMed: 26224052]

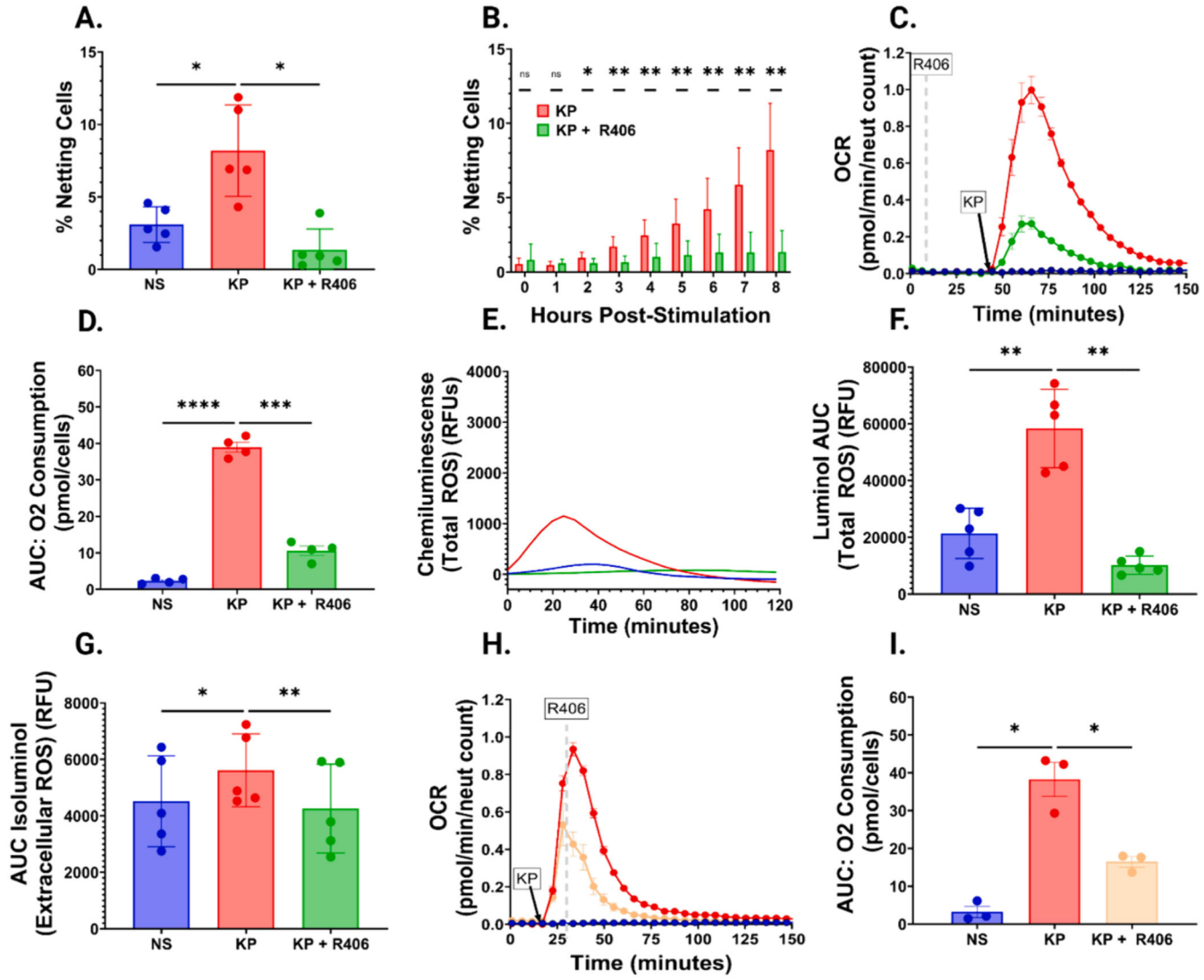

Fig. 1. R406 effectively inhibits LPS mediated NETosis and ROS generation.

(A) Bar chart comparing the percentage of non-stimulated cells (NS), K. *pneumoniae* LPS (5 μg/mL) stimulated cells (KP), or K. *pneumoniae* LPS (5 μg/mL) stimulated cells preincubated with 1 μM R406 (KP+R406) at the conclusion of eight-hour stimulation. All P values calculated utilizing the one-way ANOVA described previously unless stated otherwise. (B) Stacked bar chart comparing the percentage of KP vs KP+R406 neutrophils undergoing NETosis over the course of 8 h. P-values computed using multiple paired parametric t-tests of the percentage of NETing cells every hour over the course of eight hours. (C) Representative graph demonstrating an increase in oxygen consumption rate (OCR) in cells stimulated with 5 μg/mL of K. *pneumoniae* LPS (red line) relative to cells stimulated with the same concentration of LPS plus 1 μM R406 (green line) and control non-stimulated cells (blue line). (D) Bar chart comparing the AUC of the total oxygen consumption of cells stimulated as described in (C). (E) Kinetic graph showing increases in chemiluminescence (Total ROS generation) in neutrophils stimulated with 1 μg/mL of K. *pneumoniae* LPS (red line) relative to neutrophils stimulated with the same concentration

of LPS+R406 (green line), and non-stimulated cells (blue line) from one representative experiment. (F) Bar chart comparing the total AUC of cells stimulated as described in (E). (G) Bar chart showing the total AUC of the same conditions as described as (E), with chemiluminescence representing only external ROS generation. (H) Representative graph demonstrating an increase in oxygen consumption rate (OCR) with the same conditions described in (E), with the yellow line showing cells stimulated with the same concentration of LPS plus 1 μM R406 administered 10 min after LPS stimulation. (I) Bar chart comparing total AUC across the three conditions shown in (H).

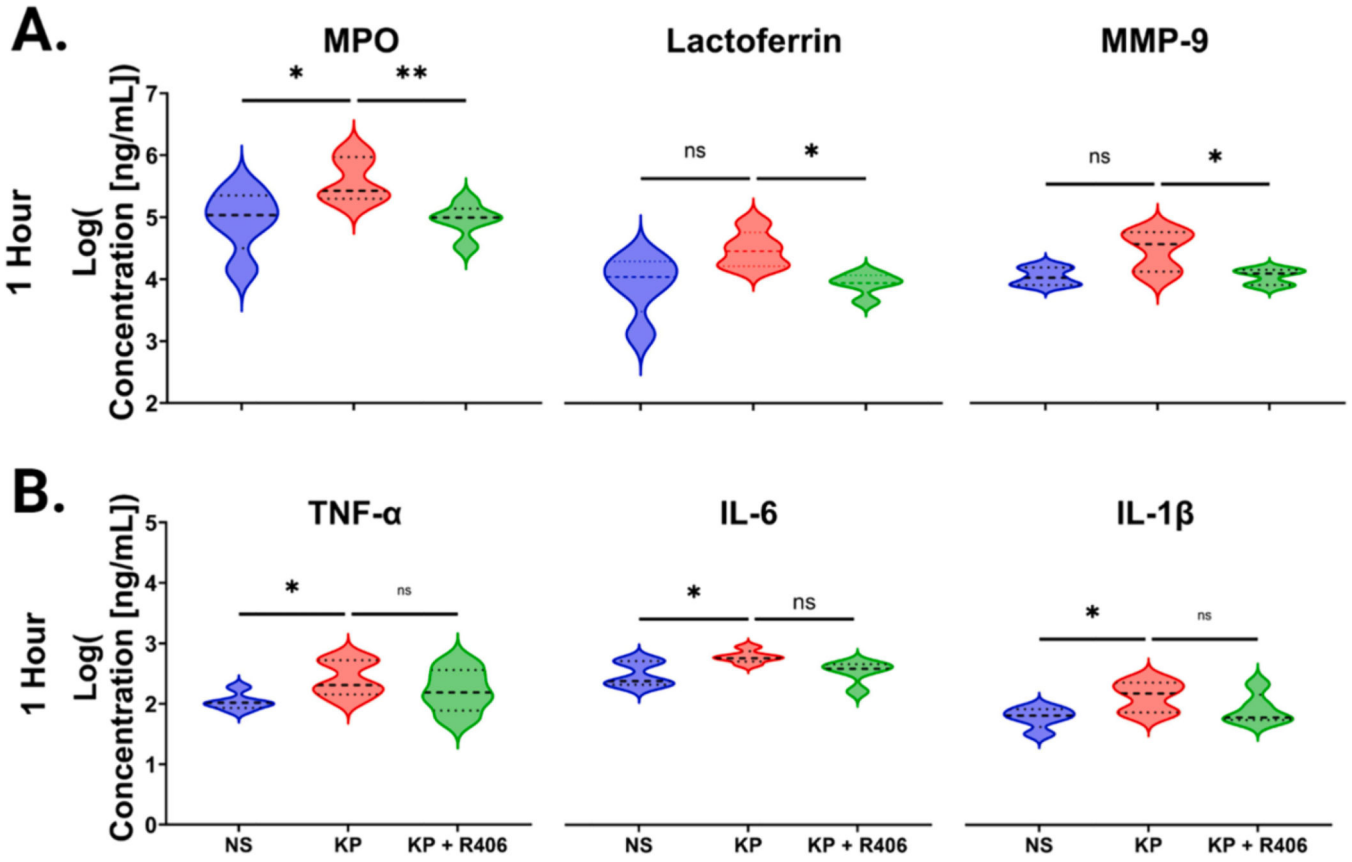

Fig. 2. R406 decreases neutrophil degranulation while having no effect on cytokine release.

(A) Volcano plots showcasing the levels of neutrophil degranulation markers, MPO, lactoferrin, and MMP9 were measured in the cell supernatant one hour post stimulation in non-stimulated cells, cell stimulated with 1 μg/mL of K. *pneumoniae* LPS, and cells stimulated with 1 μg/mL of K. *pneumoniae* LPS plus 1 μM R406. Dotted lines represent the median as well as 25th and 75th quartile for each analyte. P values were computed using one-way ANOVA for all comparison. (B) Volcano plots showcasing the concentration of soluble TNF-α, IL6, and IL-1β in the supernatant 1 h post stimulation in the same groups as (A).

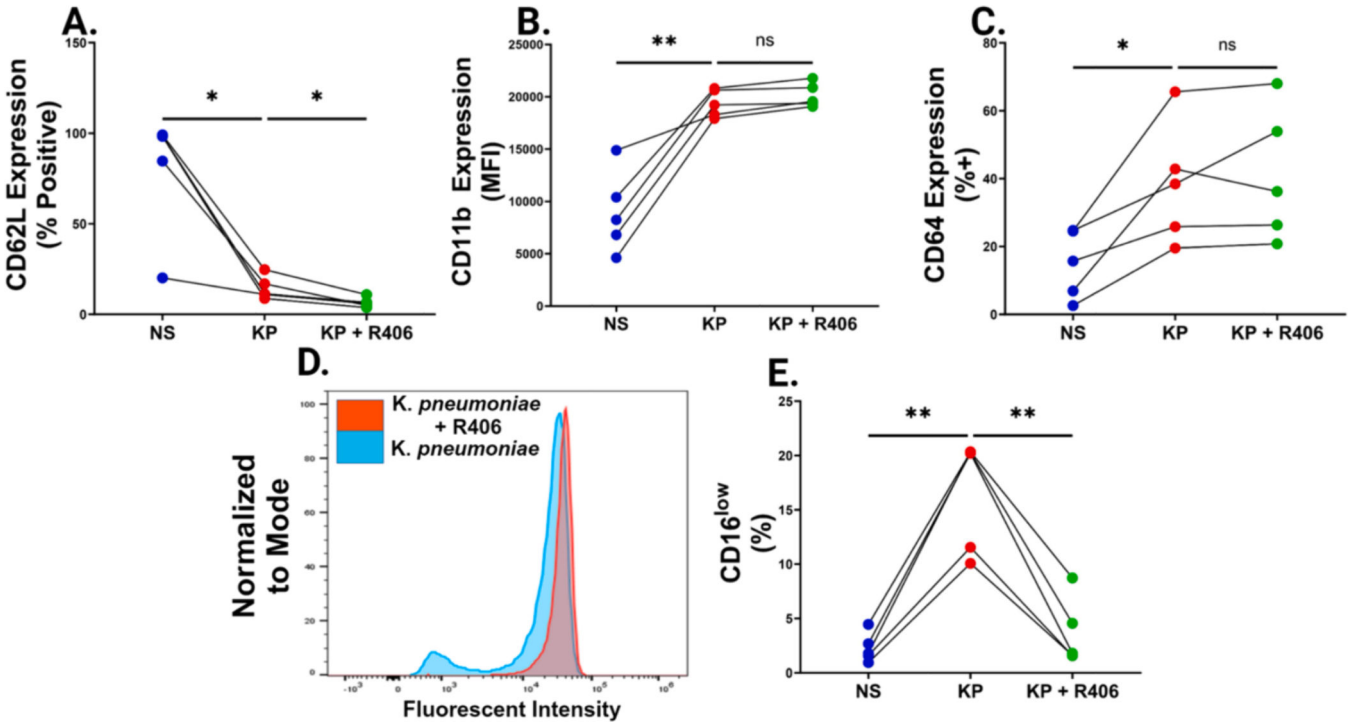

Fig. 3. R406 shows little effect on classic neutrophilic sepsis markers, but blocks CD16 shedding

(A) Paired dot plots comparing the percentage of $CD62L^{+}$ neutrophils, determined by FMO controls, one hour after stimulation in non-stimulated cells as well as cells stimulated with 1 μg/mL of K. *pneumoniae* LPS with or without 1 μM R406. All P values were determined by one way ANOVA as described previously. (B) Paired dot plots comparing the increase in CD11b Mean Fluorescent Intensity (MFI) across the same groups as described in (A). (C) Paired dot plots comparing the percentage of $CD64^{+}$ neutrophils, determined by FMO controls, in the same groups as described in (A). (D) Representative histogram showcasing the distinct $CD16^{low}$ population arising after one hour of K. *pneumoniae* stimulated neutrophils (blue) that is absent in cells preincubated with 1 μM R406 (red). (E) Paired dot plots comparing the percentage of $CD16^{low}$ neutrophils in the same groups as described in (A).

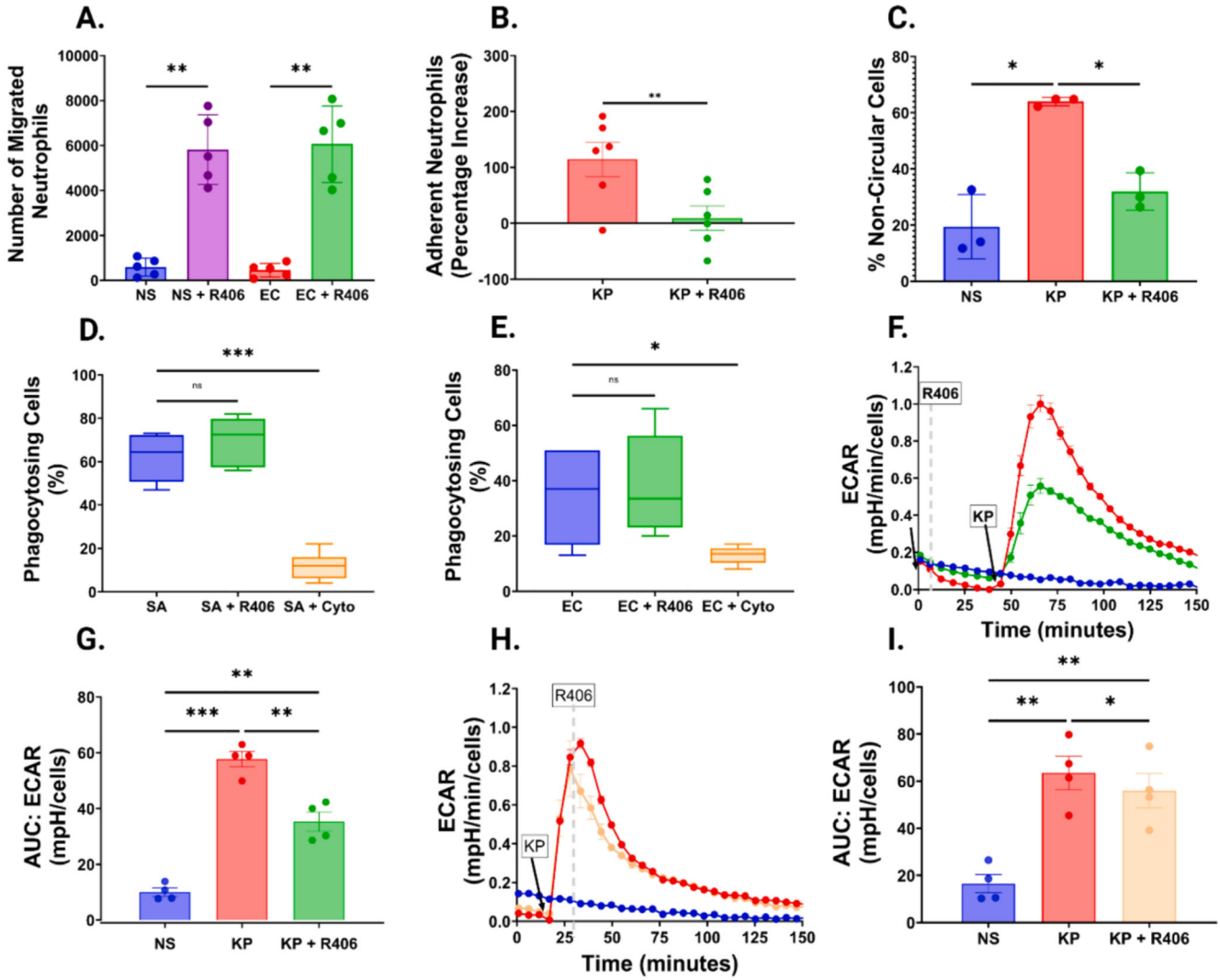

Fig. 4. R406 has diverse effects on neutrophil migration, adhesion, shape, phagocytosis, and metabolism.

(A) Bar graph showing the number of neutrophils migrating over one-hour in response to IL-8. Neutrophils were either not stimulated (NS) or exposed to 10 ng/mL E. coli (EC) LPS, with or without preincubation with 1 μM R406. All P values were computed by one-way ANOVA as previously described. (B) Bar graph comparing the percentage increase of neutrophils adhered to HUVEC cells relative to non-stimulated cells in cells stimulated with 100 ng/mL of K. *pneumoniae* LPS with or without preincubation with 1 μM R406. (C) Bar graph showcasing the percentage of non-circular cells, in non-stim cells (NS), and cells stimulated with 1 μg/mL K. pneumoniae LPS with or without R406. (D) Box and whisker graph showcasing the percentage of total cells undergoing phagocytosis Cells were either incubated with 1 μg of pHrodo® Green Staphylococcus *aureus* (SA) bioparticles either with (SA+R406) or without (SA) preincubation with 1 μM R406 or 10 μg/mL of Cytochalasin D (SA+Cyto), Boxes show mean value as well as 25th and 75th percentile of data. Whiskers represent minimum and maximum of each data set. (E) Box and whisker plot showing percentage of cells undergoing phagocytosis as shown in (D), but neutrophils were

plated with 1 μg of pHrodo® Green E. coli bioparticles. (F) Representative kinetic graph showcasing the increase in the extracellular acidification rate of the media surrounding neutrophils as measured by the Agilent Seahorse in cells stimulated with 5 μg/mL of K. *pneumoniae* LPS (red line) relative to cells stimulated with the same concentration of LPS plus 1 μM R406 (green line) and a control non-stimulated cells (blue line). (G) AUC of extracellular acidification rate of the conditions outlined in (F). (H) Representative kinetic graph showcasing the increase in the extracellular acidification rate of the media as described in (F), with the yellow line representing cells stimulated with 5 μg/mL of K. *pneumoniae* LPS followed by 1 μM R406 exposure 10 min post stimulation. (I) AUC of extracellular acidification rate of the conditions outlined in (H).